IEEE Access
Multidisciplinary | Rapid Review | Open Access Journal

Received May 19, 2022, accepted June 1, 2022, date of publication June 8, 2022, date of current version June 13, 2022.

Digital Object Identifier 10.1109/ACCESS.2022.3180732

Mosaic Based Optimization of NRD Guide Devices Using Binary Evolutionary Approaches and 2D-FVFEM

TAHIR BASHIR[1], (Graduate Student Member, IEEE), KEITA MORIMOTO[2], (Member, IEEE), AKITO IGUCHI[1], (Member, IEEE), YASUHIDE TSUJI[1], (Senior Member, IEEE), AND TATSUYA KASHIWA[3], (Senior Member, IEEE)

[1]Department of Information and Electronics Engineering, Muroran Institute of Technology, Muroran 050-8585, Japan
[2]Department of Electronics and Computer Science, University of Hyogo, Himeji 671-2280, Japan
[3]Department of Information and Communication Engineering, Kitami Institute of Technology, Kitami 090-8507, Japan

Corresponding author: Yasuhide Tsuji (y-tsuji@mmm.muroran-it.ac.jp)

This work was supported by the Japan Society for the Promotion of Science (Japan) KAKENHI under Grant 21K04169.

ABSTRACT In this paper, efficient optimal design approaches based on mosaic optimization concept are developed for NRD guide devices to realize the high-performance compact millimeter-wave integrated circuit. Binary representation-based genetic algorithm, differential evolution algorithm, harmony search algorithm, firefly algorithm, and particle swarm optimization are developed to efficiently optimize the pixel pattern in the design region of NRD guide devices. To demonstrate the usefulness of these population-based optimizations, a comparative study based on the problem-solving success rate is conducted first. To carry out this study, four NRD circuit components are designed which include low crosstalk waveguide crossing, T-branch power splitter, bending waveguide, and frequency demultiplexer. The proposed optimal devices achieve high transmission efficiencies greater than 99.9%, 49.9%:49.9%, 99.9% at 60 GHz and 96.4%, 98.5% at 59 GHz and 61 GHz. In addition, the same NRD guide components except frequency demultiplexer are also designed at wideband operation and achieve broad bandwidth around 5 GHz, 4 GHz, and 3 GHz. In order to improve the computational efficiency, the originally developed two-dimensional full vectorial finite element method is employed for the numerical simulations. This paper demonstrates the detailed implementation procedure of developed evolutionary approaches for the material distribution in the design region of NRD guide devices, comparative study of developed optimization approaches, and proposed highly attributed NRD circuit components for the realization of NRD based high-performance compact millimeter-wave circuit.

INDEX TERMS Genetic algorithm, particle swarm optimization, differential evolution, harmony search, firefly algorithm, full-vectorial finite element method, non-radiative dielectric waveguide (NRD guide).

I. INTRODUCTION

The use of millimeter- and terahertz-wave bands is being actively explored to increase communication system capacity and meet modern communication requirements. Non-radiative dielectric (NRD) waveguide technology has received a lot of attention in recent years due to non-radiative and low loss nature. Several NRD guide components have been reported so far for microwave and millimeter-wave circuit system applications. At 50 GHz, the dispersion characteristics, transmission loss, coupling coefficient, and measurement setup with several NRD-based circuit components, including T-junction, right angle corner, 90° and 180° bends, and directional coupler, are reported [1]. An NRD-based T-junction with a dielectric stub and thin metal patches with an output power of around −4 dB at 35 GHz has been proposed [2]. The coupling theory was used to analyze the losses in NRD bends (90° and 180°) at 50 GHz, with bending loss less than 0.3 dB has been presented [3]. Following a detailed examination of operational principles, propagating modes, losses, behavior of transmitting waves in bending structures, practical significance,

The associate editor coordinating the review of this manuscript and approving it for publication was Rocco Giofrè.

and the confirmation of NRD as a low-loss guide in [1]–[3], the authors proposed several NRD circuit elements at an operating frequency of 35 GHz, including a matched terminator, directional coupler, circulator, beam lead diode, gun diode oscillator, transmitter, and receiver. At 50 GHz, an NRD guide filter, a four-way power divider, and an NRD leaky-wave antenna were fabricated [4].

In millimeter-wave and terahertz applications, a substrate integrated non-radiative dielectric waveguide (SINRD) for printed circuit boards has been developed [5]. The hybrid planar non-radiative waveguide is presented and confirmed as a building block for millimeter-wave circuits, with an experimental prototype based on hybrid technology that includes active and passive components. This novel technique will be greatly useful in the development of future millimeter-wave integrated circuit systems [6]. Using mode coupling theory, a technique for designing circular and racetrack-shaped NRD guiding ring resonators was successfully devised, and a low loss, small-sized ring resonator with radii less than 3.5 mm was built at 60 GHz with band rejection performance of more than 30 dB [7]. At a frequency of 77 GHz, a new sort of NRD-based directional coupler using two separate NRD guides interconnected with a bridge is presented and fabricated [8]. At 60 GHz, a first tunable liquid crystal filter based on NRD technology is presented, with fractional bandwidth and tunability of 1% and 2.5%, respectively [9]. Furthermore, over the tuning range, the filter insertion loss ranges between 4.9 and 6.2 dB.

Many additional research for the development of NRD waveguide theory and circuit components for millimeter application were presented in the literature. Some of them have already been addressed above, while the rest are listed in Table 1 [10]–[33]. In this comprehensive evaluation, all NRD circuit components are proposed without employing optimization approaches for NRD guiding structures. It is well understood that without optimization, a high-performance compact millimeter-wave integrated circuit is not viable. For this purpose, we developed several optimization approaches to optimize the design region of NRD guide devices. In this regard, our proposed research work is unique and distinct from the existing literature on NRD waveguide technology.

Several optimization approaches and variants based on size, shape, topology, and mosaic optimization concepts, such as genetic algorithm, particle swarm optimization, inverse design algorithm, and direct binary search algorithm, have been proposed for the efficient design of optical, dielectric, and photonic crystal guide devices [31]–[50]. However, a study about the development of optimal design approaches using the above-mentioned optimization concepts for NRD guides is insufficient and still has great potential in this domain. In the literature and to the authors best knowledge the development of binary evolutionary approaches based on mosaic optimization concepts, detailed implementation procedure, comparative study, and high performance NRD circuit components at single frequency operation and broadband operation, has not been proposed previously and it is also verified from Table 1.

In this paper, in order to add the valuable contributions in NRD platform, we develop several optimization approaches for the efficient design of NRD guide components with various functions to realize the high-performance compact millimeter-wave circuit as depicted in Fig. 1. For this purpose, digital material concept (mosaic-optimization) using binary evolutionary approaches is very useful. Using mosaic-based optimization a small number of variables are used to express the design region of NRD guide and those variables are optimized by five optimization approaches which include binary-representation-based genetic algorithm (GA), differential evolution algorithm (DEA), harmony search algorithm (HSA), firefly algorithm (FA), and particle swarm optimization (PSO). To find the most efficient ones, a comparative study based on problem-solving success rate (also known as convergence rate) is carried out first, using four numerical examples: low crosstalk waveguide crossing, T-branch power splitter, and bending waveguide at 60 GHz, as well as frequency demultiplexer at 59 GHz and 61 GHz. In addition, same NRD guide components except frequency demultiplexer are also designed by modifying the objective function for broadband operation. In modified objective function we used several frequency intervals within desired frequency band for each generation of optimization method. On other hand, to improve the design efficiency originally developed two-dimensional full-vectorial finite element method (2D-FVFEM) is used for the numerical simulation of NRD guide devices [51]. Our 2D-FVFEM is verified by 3D-FVFEM using several optimal and non-optimal NRD guide structures [18]–[20].

The paper is organized as follow: The brief discussion of NRD guide and structure representation using mosaic-based optimization are presented in section II. The evolutionary approaches for binary optimization and the brief discussion of BGA, BDEA, BHSA, BFA, and BPSO are described in section III. The simulation results of numerical design examples of NRD guides are described in section IV. Conclusion of this research work is in section V.

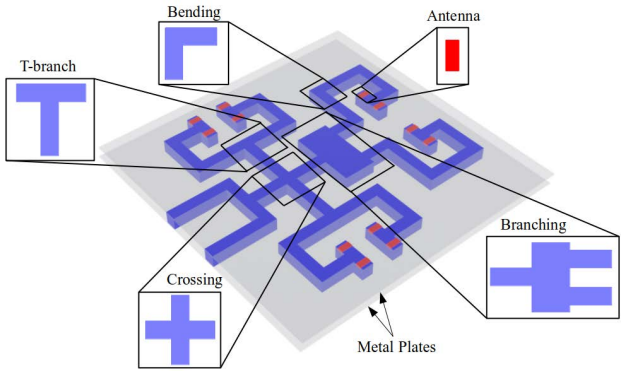

FIGURE 1. Image of NRD based millimeter-wave circuit.

TABLE 1. Comprehensive review of NRD guide devices and design strategy.

Ref.	Freq. [GHz]	Devices	Optimization
[1]	50	T-junction 90° bend 180° bend Directional coupler	—
[2]	35	T-junction	—
[3]	50	90° bend 180° bend	—
[4]	35, 50	Match terminator Directional coupler Circulator Beam lead diode Gun diode oscillator Transmitter Receiver Filter Power divider Leaky-wave antenna	—
[5]	70	SINRD waveguide	—
[6]	20, 19.65, 16	Microstrip transition Bandpass filter Planar NRD oscillator	—
[7]	60	Ring resonator	—
[8]	77	Directional coupler	—
[9]	60	Liquid crystal filter	—
[10]	60	Mixer using bandpass filter	—
[11]	60	Flexible transmission line	—
[12]	60	Beam lead diode	—
[13]	77	Amplitude shift keying Phase shift keying	—
[14]	60	Transmitter and receiver	—
[15]	60	ASK Transceiver	—
[16]	60	High speed transceiver	—
[17]	60	Guide duplexer	—
[18]	60	90° bend	DBSA
[19]	60	Crossing and T-branch guide	DBSA, GA
[20]	Broadband	Crossing T-branch 90° bend Z-bend guide	BGA
This work	Wideband	Waveguide crossing Power splitter Bending guide Frequency Demux. at 59 and 61 GHz	BDEA BHSA BGA BFA and BPSO

"—" means "optimization technique is not applied."

II. NRD GUIDE WITH MOSAIC-LIKE STRUCTURE

A. NRD GUIDE

NRD guide has been proposed as a millimeter waveguide by T. Yoneyama [1]. As illustrated in Fig. 2(a), its structure is made up of dielectric sandwiched between metal parallel plates with spacing less than $\lambda/2$ to realize the non-radiative nature. In NRD guide, propagation loss is relatively small because most of the electromagnetic energy flows through the dielectric and air and a very small amount of current flow in the metal plates. Usually, NRD guide support two orthogonal modes such as LSM_{01} and LSE_{01} mode. For LSM_{01}, the electric field is parallel to the metal plate whereas in LSE_{01} mode, the electric field is perpendicular to the plate as shown in Fig. 2(b). Both modes are non-radiative in nature and cannot propagate within air region sandwiched metal parallel plates and can be used as a non-radiative waveguide. LSM_{01} mode

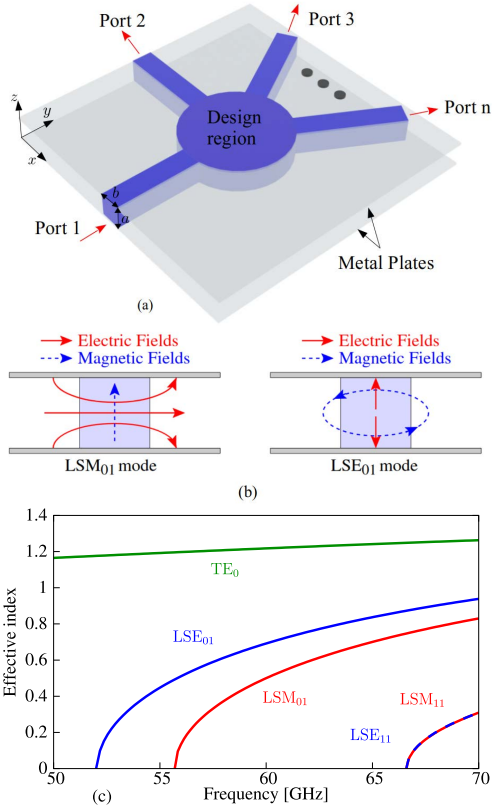

FIGURE 2. (a) an image of NRD guide, (b) propagation modes, and (c) dispersion relation a = 2.25 mm, b = 2 mm, $\varepsilon_r = 2.2$.

whose polarization is parallel to the metal is usually used in NRD guide, in contrasted to microstrip line which supports polarization perpendicular to the metal. Furthermore, the dispersion relation of NRD guide is also calculated as shown in Fig. 2(c).

B. STRUCTURE REPRESENTATION OF NRD GUIDE USING MOSAIC-BASED OPTIMIZATION

Achieving the desired properties typically requires many design variables to optimize material distribution in the target area of the guide device. Several optimization approaches have been proposed to optimize these variables, using various optimization concepts such as shape, size, and topology optimization. In which, size optimization deals with dimensional parameters such as the length and width of the structure, whereas shape optimization optimizes the outer shape of the structure, and the topology optimization optimizes the material distribution within area of interest. On other hand, mosaic-based optimization is another way to efficiently optimize the guide devices. Mosaic structures show the presence of dielectric materials in the form of pixels at particular positions within the area of interest.

In this work, mosaic-based optimization using evolutionary approaches is considered to optimize the material distribution in the design region of NRD guide. Several design variables are employed to express material distribution in the design region. In order to create a mosaic-like structure,

first discretize the design region into a grid pattern and then allocate a dielectric or air to each pixel (also known as a mosaic) in the form of 1 or 0, respectively as shown in Fig. 3. This is called the concept of digital materials. The degree of design freedom of our optimization approaches is determined by the number of pixels. A large number of pixels may make it difficult to fabricate a designed device. The pixel size is determined not by the convenience of the optimization method, but by the possibility of fabrication. A brief description of implementing the optimization approaches is given below in the next section.

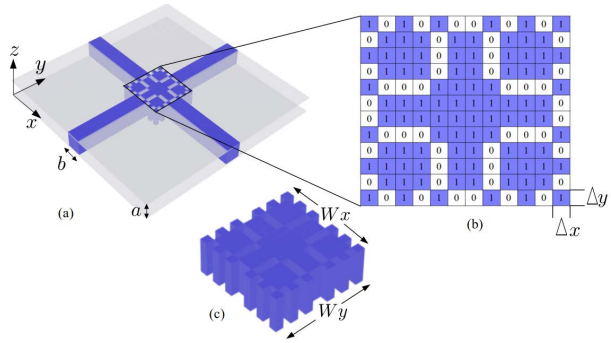

FIGURE 3. Non radiative dielectric (NRD) waveguide (a) design setup (b) representation of design region using mosaic-based optimization concept (c) example of optimized design region.

III. EVOLUTIONARY APPROACHES FOR BINARY OPTIMIZATION

In evolutionary approaches, three processes are involved in the evolution of the population. The first step is initialization, which involves randomly generating an initial population of individuals based on a predetermined quantity. Determining an appropriate population size and individual representation technique that are more likely to offer feasible solutions are important. Another important parameter is the number of iterations. Both the population size and the number of iterations may have a significant impact on solution quality and time. After a few trials, an appropriate selection of these parameters can be determined based on the design problem resulting in a feasible solution. Individuals can be represented using a variety of ways, including binary representation, real value representation, and integer value representation.

The second step is to calculate the value of each individual using a problem-dependent objective function after the population has been randomly generated. The calculated value can be used to rank each individual for selection purposes. Whether the breaking criteria has been satisfied is judged after the evaluation of objective function. Different breaking criteria, such as static, dynamic, and hybrid, are used to stop the optimization process. When dynamic criteria is used, the optimization is executed until the desired characteristics is achieved, whereas the optimization is terminated at a fixed number of iterations in the case of static criteria. A combination of these two criteria is called a hybrid and is used in some cases. If no individual satisfies the desired property, the third stage of the evolutionary technique generates a new population by perturbation of solutions in the existing population. In evolutionary approaches, three processes are involved in the evolution of the population. The generic optimization procedure of our binary evolutionary approaches that we considered in this paper is shown in Fig. 4.

In this paper, the size of population (Np = 64) is same for all evolutionary approaches. The starting search point is varies from one another due to the random generation of populations, resulting in differing optimal structures. The number of iterations required may be determined by the device function, whether it is designed for single-frequency operation or wideband operation. For single and broadband operation, we evaluated a maximum of 100 and 300 iterations for all devices, respectively. Binary representation is considered to represent an individuals structure because the digital material concept is employed to generate a mosaic-like structure. The optimization process is terminated by using static breaking criteria.

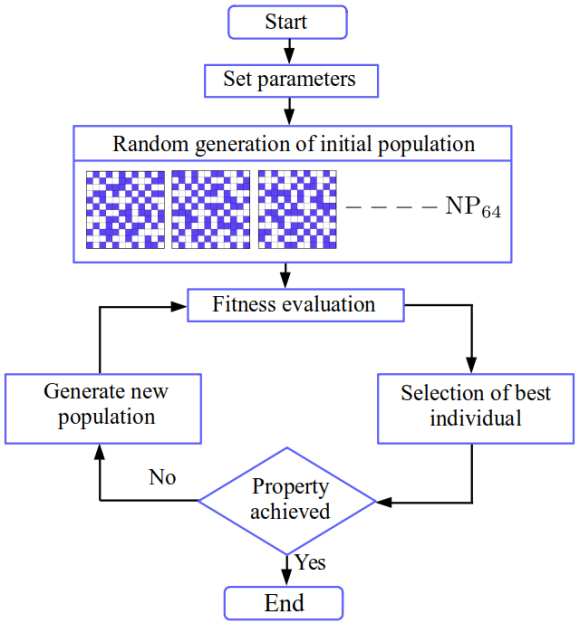

FIGURE 4. Generic work procedure of binary evolutionary methods.

A. BINARY GENETIC ALGORITHM (BGA)

John Holland proposed GA, a metaheuristic global search-optimization method, in 1975 [52]. Conventional GA and its variants are used to solve a wide range of complex optimization problems. The basic goal of GA is to simulate natural selection and survival of the fittest individuals. In GA, the procedure starts with a randomly generated initial population. Each individual in population is a solution set or chromosome, which is encoded using digital material techniques. After the population is randomly generated, each individual is evaluated using a problem-dependent objective function and ordered from best to worst based on the calculated value. GA is a method for generating new populations that mimics

natural selection of individuals, and it employs three biologically inspired operators: selection, crossover, and mutation. The developed optimization method considers two different selection techniques. To save the best individual from the entire population, first elite selection is used. On the other hand, rank selection, is used to select the best individuals for a new generation. Once the parent individuals $\boldsymbol{x}_{p1}^{(n)}$ and $\boldsymbol{x}_{p2}^{(n)}$ are selected, the crossover operator perturbs the selected individuals to produce new offspring as follows:

$$x_{c,k}^{(n+1)} = \begin{cases} x_{p1,k}^{(n)} & U(0,1) \leq 0.5 \\ x_{p2,k}^{(n)} & \text{otherwise} \end{cases} \tag{1}$$

where $U(0, 1)$ is a random number between 0 and 1 and $x_{i,k}^{(n)}$ denotes k-th component of the design variable vector $\boldsymbol{x}_i^{(n)}$. After crossover, the newly generated offspring have a tendency to become highly similar to previously selected individuals, reducing population diversity and perhaps leading to population stagnation. The bit flip mutation operator is employed to inject diversity into the population to avoid stagnation. With this optimization approach, the mutation rate is 1%. The evolution of a randomly generated population is now complete. This search process is repeated until the number of iterations is reached. Finally, the best individual at the final iteration will be the optimal mosaic-like structure of the NRD guide.

B. BINARY DIFFERENTIAL EVOLUTION ALGORITHM (BDEA)

DEA is a metaheuristic optimization approach, and first proposed by Storn and Price in 1995 for global optimization [53]. Usually, DEA performs better than GA because it explores the given search space more efficiently, when multi objectives are need to be optimized. The key reasons for differential evolution application in electromagnetic optimization are its reliability in dealing with multi-minima functional and its improved rate of convergence as compared to GA when applied to small scale real valued problem. It is critical to improve the candidate solution with each iteration, and it doesn't require explicit cost function gradients in the candidate solution search space. As a result, DEA can be applied to problems that are not even continuous or non-differentiable. The most important feature of DEA is its unique mutation operation. The scaling parameter S and the population size N_P are two critical control parameters in DEA. The key steps in the implementation of DEA are mutation, crossover, and selection. First, in binary strategy, a mutant individual is generated as follows:

$$x_{m,k}^{(n)} = \begin{cases} x_{p1,k}^{(n)} + (x_{p2,k}^{(n)} - x_{p3,k}^{(n)}) & U(0,1) < S \\ x_{p1,k}^{(n)} & \text{otherwise} \end{cases} \tag{2}$$

where $x_{m,k}^{(n)}$ is a mutant individual and may possible to take the value of other than binary number -1 or 2 if the values of randomly selected individuals are $(x_{p1,k}^{(n)}, x_{p2,k}^{(n)}$, and $x_{p3,k}^{(n)}) =$ (0, 0, 1) or (1, 1, 0) respectively. In order to binarize the mutant individual the value of $x_{m,k}^{(n)}$ is set to be (0, 1) as follow.

$$x_{m,k}^{(n)} = \begin{cases} 0 & (x_{m,k}^{(n)} < 0.5) \\ 1 & (\text{else}) \end{cases} \tag{3}$$

The scaling parameter S is used to control the differential variations and it is set to be 0.75. The operation described above is called the mutation of DEA. The second step of DEA is crossover. In DEA, $\boldsymbol{x}_t'$ is the candidate of next generation by crossover between mutant individual $\boldsymbol{x}_m^{(n)}$ and target individual $\boldsymbol{x}_t^{(n)}$.

$$x_{t,k}' = \begin{cases} x_{t,k}^{(n)} & (U(0,1) < 0.5) \\ x_{m,k}^{(n)} & \text{otherwise} \end{cases} \tag{4}$$

Then $\boldsymbol{x}_t'$ is used as $\boldsymbol{x}_t^{(n+1)}$ if $\boldsymbol{x}_t'$ is better than $\boldsymbol{x}_t^{(n)}$, otherwise $\boldsymbol{x}_t^{(n)}$ is restored. The third step of DEA is to select the best individual between target individual and candidate individual for next round until the completion of iteration.

C. BINARY HARMONY SEARCH ALGORITHM (BHSA)

HSA is a population-based metaheuristic optimization approach proposed by Geem *et al.* in 2001 [54]. HSA is inspired by the improvisation process of experienced musicians. The key benefits of HSA are its clarity of execution, record of success, and ability to solve a variety of complex problems. Pitch adjustment rate, bandwidth, and harmony memory considering rate are the three main parameters that control exploitation and exploration in HSA. Through the selecting and tuning process, a new harmony is created in HSA. Each design variable is chosen from the harmony memory, which contains previous good harmonies. A random number, with a specified probability, tunes or replaces the selected harmony. The new harmony $\boldsymbol{x}_h^{\text{new}}$ is generated as follows:

$$\begin{aligned} x_{m,k} &= x_{p1,k} + x_{p2,k} + x_{p3,k} \\ x_{h,k}^{\text{new}} &= \begin{cases} (U(0,1) < 0.5)?\ 0 : 1 & (C_h < (1 - R_{\text{hmcr}}) \\ (x_{m,k} = 0 \text{ or } 2)?\ 0 : 1 & (C_h < (1 - R_{\text{hmcr}}) \\ & \qquad (1 + R_{\text{par}}) \\ (x_{m,k} \leq 1)?\ 0 : 1 & \text{otherwise} \end{cases} \end{aligned} \tag{5}$$

where $C_h = U(0, 1)$ and $x_{m,k}$ is k-th sound generated in considering harmony memory. R_{hmcr} is the harmony memory considering rate (HMCR), and it is utilized to make the harmony memory more effective. If the HMCR value is very low, close to 0, only a few harmonies are used, and therefore the convergence rate is slow, whereas large rates exploit the harmonies, and the solution space is not fully explored, thus leading to an insufficient solution. The value of HMCR should be in the range of 0.7-0.95. In this optimization approach the $R_{\text{hmcr}} = 0.85$ has been set. The pitch adjustment rate R_{par}, is used to control the degree of adjustment. Because of the limitation in exploring only a small subspace of the entire subspace, a small R_{par} with narrow bandwidth can slow down HSA convergence, whereas a large R_{par} with a wide

bandwidth can lead to optimization deviation in some optimal solutions. In this optimization approach, the pitch adjustment rate is set to be $R_{\text{par}} = 0.2$.

D. BINARY PARTICLE SWARM OPTIMIZATION (BPSO)

PSO is an iterative optimization approach that takes its inspiration from the animal kingdom, specifically a group of animals moving in search space for common objective. Dr. Eberhart and Dr. Kennedy were the first to suggest PSO [55]. In PSO, a swarm of particles is the first to be randomly initialized. Each particle has its own unique position and velocity. Each particle changes its position continuously inside a specified search space with velocity to find the optimal location. The particles movement is determined by its memory path and iteration with other particles. The best position of each particle and the best position of the swarm are updated once all particles have reached the new place. PSO finds the best solution by collaborating and sharing information among swarm particles. The following are the steps in the PSO procedure:

1. Generate an initial swarm with initial position and velocity.
2. Evaluate objective function of each particle.
3. Update both the individual and global best positions.
4. Update each particle velocity and position.

The optimization process is repeated until the termination criterion is met. The following equations are used in PSO to update the position and velocity of the particles.

$$\boldsymbol{y}_i^{(n+1)} = \boldsymbol{y}_i^{(n)} + \boldsymbol{v}_i^{(n+1)} \tag{6}$$

$$\boldsymbol{v}_i^{(n+1)} = W\boldsymbol{v}_i^{(n)} + C_1 r_1(\boldsymbol{y}_p^{(n)} - \boldsymbol{y}_i^{(n)}) + C_2 r_2(\boldsymbol{y}_g^{(n)} - \boldsymbol{y}_i^{(n)}) \tag{7}$$

$$\boldsymbol{x}_i^{(n+1)} = \text{binarize}(\boldsymbol{y}_i^{(n+1)}) \tag{8}$$

where $\boldsymbol{y}_i^{(n)}$ and $\boldsymbol{v}_i^{(n)}$ are the position and velocity of i-th particle respectively, while $\boldsymbol{y}_p^{(n)}$ and $\boldsymbol{y}_g^{(n)}$ are the individual and global best positions of n-th iteration respectively. W is the inertial weight parameter with a value 0.8 that adjusts the ability to search locally and globally. The initial cognitive and social cognitive coefficients, C_1 and C_2 can adjust the balance between individual and global optimum positions. r_1 and r_2 are two random values between 0 and 1 which are used to simulate the random components of swarm behavior. To obtain $\boldsymbol{x}_i^{(n+1)}$, the following binarization scheme is employed:

$$x_{i,k}^{(n+1)} = \begin{cases} 1 & \left(\dfrac{1}{1+\exp(-y_{i,k}^{(n+1)})} + \Delta U(-1,1) > 0.5\right) \\ 0 & \text{otherwise} \end{cases} \tag{9}$$

where Δ is a coefficient introduced to avoid being trapped in a local solution and is set to be $\Delta = 0.125$.

E. BINARY FIREFLY ALGORITHM (BFA)

FA is a swarm-based metaheuristic optimization algorithm first proposed by Xin She Yang in 2008 [56]. FA is inspired by the movement of fireflies as they interact based on their flashing light. Regardless of their gender, particles are attracted to others because of their attractiveness. Attractiveness is determined by brightness and distance between them. The optimization process of FA consists of three steps. First, a particles called fireflies are randomly generated. Each firefly has a brightness level. The brightness is used to calculate the value of each firefly by using objective function. For minimization problem, the fireflies with small value are more brighter than higher ones. Once brightness of fireflies is evaluated, then fireflies follow those ones who are rich in brightness. The brightest firefly conducts a local search by moving randomly in its surroundings. The position of firefly $\boldsymbol{y}_i^{(n)}$ is updated by equation as follow:

$$\boldsymbol{y}_i^{(n+1)} = \boldsymbol{y}_i^{(n)} + \sum_j u(\beta_{(0,j)} - \beta_{(0,i)})\beta_{(0,j)} e^{-\gamma r_{ij}^2} \times (\boldsymbol{y}_j^n - \boldsymbol{y}_i^n) + \alpha\delta^n \boldsymbol{\varepsilon} \tag{10}$$

$$\boldsymbol{x}_i^{(n+1)} = \text{binarize}(\boldsymbol{y}_i^{(n+1)}) \tag{11}$$

The attraction to the brighter neighbor is calculated using the second term of the above equation where, $\beta_{(0,j)}$ is attractive force of the j-th particle and r_{ij} is a distance between i-th and j-th particles. $u(\xi)$ is the unit step function. $\boldsymbol{y}_i^{(n)}$ and $\boldsymbol{y}_j^{(n)}$ are the positions of fireflies at n-time. The light absorption coefficient of medium is $\gamma = 1/\sqrt{L}$ and L is used to adjust the search range of particles. The third term in the above equation is for randomization, where α is the scaling factor used to adjust the random step length, δ is the damping factor and $\boldsymbol{\varepsilon}$ is a random vector. The values of δ and α are 0.99 and 0.25, respectively. Using the above equation, the firefly's position is updated before the end of iterations.

IV. DESIGN EXAMPLES OF NRD GUIDE

In this paper, we proposed the concept of realizing a high-performance millimeter-wave integrated circuit using basic NRD guide components as shown in Fig. 1. Evolutionary approaches have been developed to obtain the optimal design of the NRD guides. To demonstrate the usefulness of these optimization approaches, we considered four numerical examples of NRD guide devices. Except symmetrical conditions in design region, size of design region, position and number of output ports, the other basic geometrical parameters are the same in all devices. In our design examples, we assume the spacing between metal plates is $a = 2.2$ mm, length and width of the dielectric strip are $l = 10$ mm and $b = 2$ mm, respectively. The relative permittivity of dielectric and air is $\varepsilon_r = 2.2$ and $\varepsilon_{\text{air}} = 1.0$ respectively. The size of design region in waveguide crossing, T-branch power splitter and bending waveguide is $W_x = W_y = 6$ mm and it is discretized into 144 pixels. In case of frequency demultiplexer $W_x = 6$ mm and $W_y = 16$ mm with total 384 pixels in the design region. The size of each pixel is 0.5 mm × 0.5 mm that is quarter of the dielectric strip. In order to make the fabrication feasible, pixel size is determined by considering the operating wavelength, guide width and fabrication sensitivity. The computational domain is surrounded by

a perfectly matched layer (PML) with a thickness of $d_{\text{PML}} = 5$ mm. LSM_{01} mode at 60 GHz is incident at input port 1 in first three examples. In case of frequency demultiplexer wave at two frequencies 59 GHz and 61 GHz are incident, and it is selectively output to port 2 and 3 respectively. In order to achieve the desired properties, the design region of size $W_x \times W_y$ is optimized.

A. LOW CROSSTALK WAVEGUIDE CROSSING

First, we consider low crosstalk NRD waveguide crossing as shown in Fig. 5. The geometrical parameters and incident conditions are explained above. In order to make the optimization process easy and faster, a unique one-two structural symmetric conditions are applied in the design region indicated by red line, to optimize the half design region except whole as shown in Fig. 5. The following objective function is used at 60 GHz to achieve the maximum transmission efficiency at output port 3 when LSM_{01} mode is incident at input port 1.

$$\text{Minimize } F = 1 - |S_{31}(f)|^2 \quad (\text{at } 60 \text{ GHz}) \tag{12}$$

The pixel pattern is optimized by using five different optimization that are described in section III. The convergence behavior of these optimization approaches at 60 GHz is shown in Fig. 6(a). We can see that all optimization approaches show good convergence in the range of 60 to 80 number of iterations. The performance of BHSA and BDEA is slightly better, but other optimizations also achieved sufficient device performances. Figure 7 shows the optimized structure, propagation field, and frequency characteristics of BHSA which is the best one in case of waveguide crossing at 60 GHz operation. The frequency characteristics of waveguide crossing using other optimizations are shown in Fig. 8. Due to random generation of initial population in each optimization the optimal structures are different to each other. Although, optimized structures are different but overall device performance is almost same for each design as shown in Fig. 8. All optimized waveguide crossings achieve high transmission power more than 0.95. In Fig. 7, frequency analysis by BHSA relatively show broad bandwidth characteristics. By considering this clue, we modified our objective function to realize the broadband operation possible.

In order to achieve the broader bandwidth we used the following modified objective function.

$$\text{Minimize } F = \frac{1}{3}\sum_{i=1}^{3}(1 - |S_{31}(f_i)|^2)$$
$$(f_{1,2,3} = 58,\ 60,\ 62 \text{ GHz}) \tag{13}$$

The updated objective function analyzes the waveguide structure using three different frequencies at a time for each generation of optimization approaches. Usually, a large number of iterations are required to optimize the structure for broadband operation because multiple frequencies involve in the objective function. In Fig. 6(b) we can see that how efficient our developed optimization approaches that converge the solution at broadband operation with almost same number of iterations used for single frequency operation. The optimized structure at broadband operation, propagation fields at considered frequencies in the objective function and frequency characteristic by BDEA are shown in Fig. 9. Furthermore, the performance detail of proposed NRD waveguide crossing is summarized in Table 2. By using modified objective function, all optimization approaches achieve high broadband property around 5 GHz in the frequency range of 58 GHz-63 GHz.

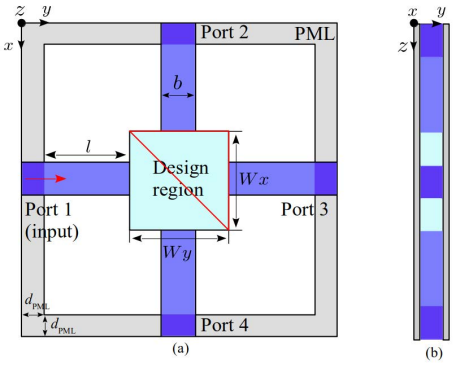

FIGURE 5. Initial structure of NRD waveguide crossing (a) top view (b) front view.

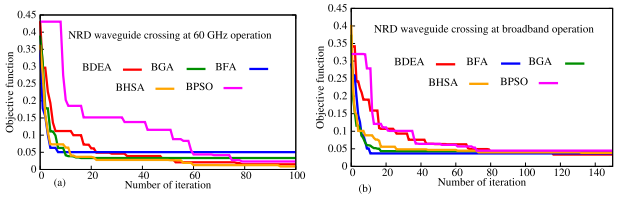

FIGURE 6. Convergence behavior of NRD waveguide crossing at (a) 60 GHz (b) broadband operation.

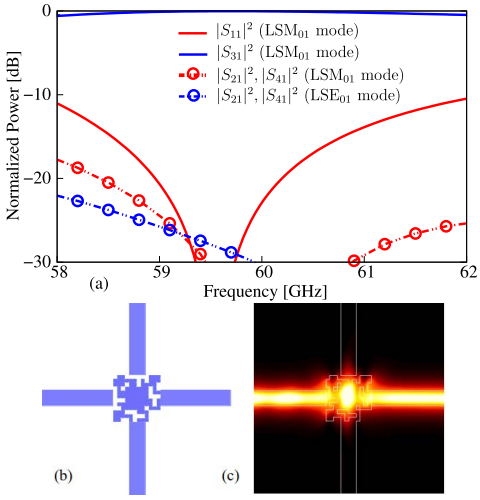

FIGURE 7. Optimal results of waveguide crossing at 60 GHz using BHSA (a) frequency characteristics, (b) optimized structure and (c) propagation field.

B. T-BRANCH POWER SPLITTER

Next, we considered second numerical example NRD T-branch power splitter as shown in Fig. 10. The geometric

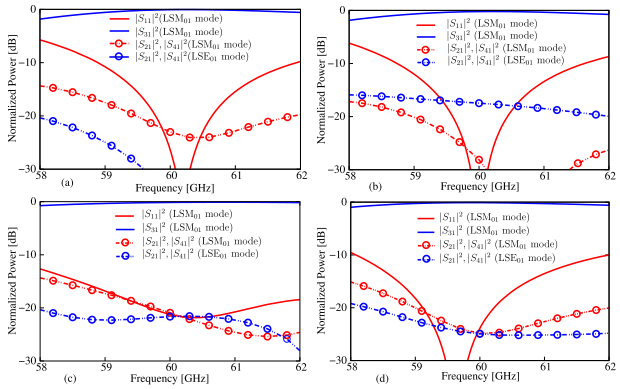

FIGURE 8. Frequency characteristics analysis of waveguide crossing at 60 GHz operation (a) BDEA (b) BFA (c) BGA (d) BPSO.

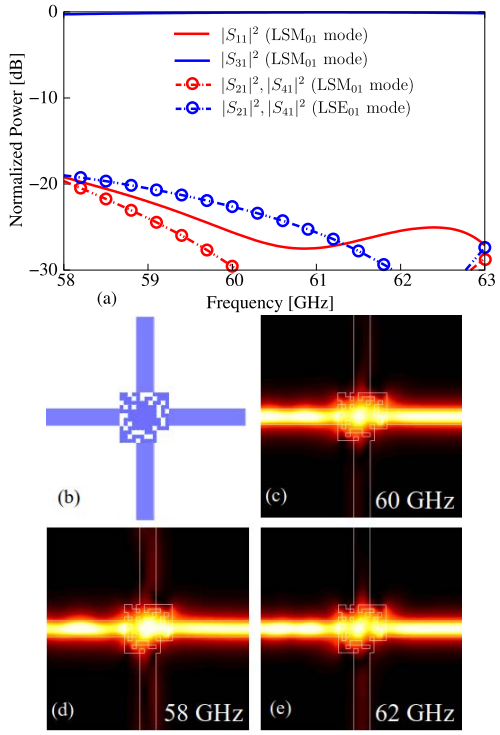

FIGURE 9. Optimal results of waveguide crossing at broadband operation using BDEA (a) frequency characteristics, (b) optimized structure and (c-e) propagation field.

parameters are the same as in the previous example, except for the number of output ports and the condition for structural symmetry. In order to split the transmission power equally at output ports, one-two symmetric condition in rectangle form is applied indicated by red line as shown in Fig. 10. Due to considered symmetry, pixels in the upper half of the design region are optimized. The following objective function is used to achieve the maximum transmission power at 60 GHz.

$$\text{Minimize } F = 1 - |S_{21}(f)|^2 - |S_{41}(f)|^2 \quad \text{(at 60 GHz)} \tag{14}$$

where $|S_{21}|^2$ and $|S_{41}|^2$ are transmission powers from port 1 to port 2 and port 1 to port 4 respectively. Figure 11(a) shows the convergence behavior of optimization approaches for

TABLE 2. Detail performance analysis of NRD waveguide crossing at 60 GHz and broadband operation.

Crossing 60 GHz	Transmission [dB]		Reflection [dB]		X-talk
	LSM_{01}	LSE_{01}	LSM_{01}	LSE_{01}	[dB]
BHSA	−0.03	−29.0	−22.8	−30.2	−50.4
BDEA	−0.06	−32.7	−26.3	−34.7	−33.8
BPSO	−0.10	−24.7	−23.8	−31.5	−32.6
BGA	−0.14	−34.6	−21.2	−24.0	−45.3
BFA	−0.22	−21.5	−53.5	−20.7	−28.1
Broadband Crossing	**Transmission [dB]**		**Rx. [dB]**	**X-talk**	**BW**
	LSM_{01}	LSE_{01}	LSM_{01}	[dB]	[GHz]
BDEA	−0.08	−31.2	−25.6	−29.5	5.0
BFA	−0.10	−37.9	−31.0	−44.9	5.0
BHSA	−0.12	−36.9	−25.5	−53.7	5.0
BGA	−0.12	−32.8	−25.5	−33.1	5.0
BPSO	−0.11	−42.2	−24.7	−53.6	5.0

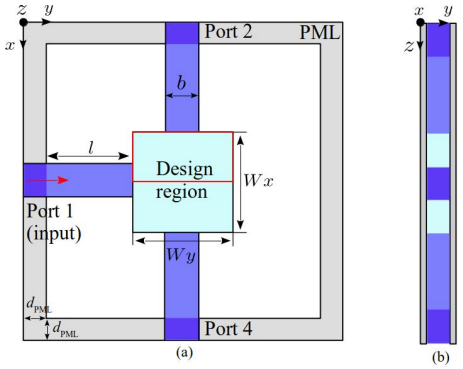

FIGURE 10. Initial structure of NRD T-branch power splitter (a) top view (b) front view.

T-branch guide at 60 GHz in which BDEA, BHSA, and BFA converge the solution very efficiently between 40 to 60 number of iterations. However, BGA requires more number of iterations for better convergence in comparison to BDEA, BHSA and BFA but it also achieves a desired device performance. The optimal structure, propagating field at 60 GHz and frequency characteristics of BHSA obtained by 2D-FVFEM are shown in Fig. 12, and it depicts that optimal structure can efficiently split the power equally into two output ports. The frequency characteristics of T-branch guide using other optimizations are shown in Fig. 13. The optimized structures by BDEA, BHSA, BGA, BPSO and BFA achieved high splitting power ratio at 60 GHz $|S_{21}|^2 = |S_{41}|^2 = 0.499, 0.496, 0.493, 0.491$, and 0.488 respectively. Based on the convergence analysis at 60 GHz we considered all optimization approaches for broadband operation by using objective function as follow:

$$\text{Minimize } F = \frac{1}{5}\sum_{i=1}^{5}(1 - |S_{21}(f_i)|^2 - |S_{41}(f_i)|^2)$$
$$(f_{1,2,3,4,5} = 58,\ 59,\ 60,\ 61,\ 62\ \text{GHz}) \tag{15}$$

In order to ensure the broad bandwidth, more close intervals within interested frequency band are considered in the objective function. Figure 11(b) show the convergence behavior at broadband operation and it shows almost same behavior and convergence order as in 60 GHz operation. In this design, BDEA, BHSA, and BGA achieved desired property around

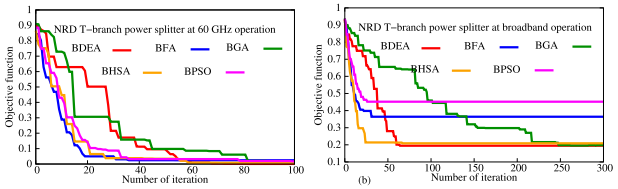

FIGURE 11. Convergence behavior of NRD T-branch at (a) 60 GHz (b) broadband operation.

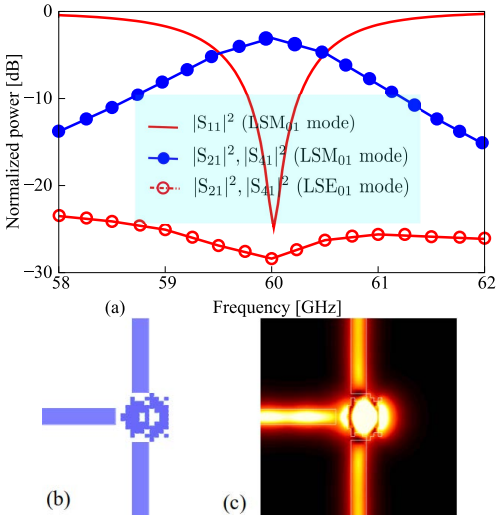

FIGURE 12. Optimal results of NRD T-branch at 60 GHz using BHSA (a) frequency characteristics, (b) optimized structure and (c) propagation field.

TABLE 3. Detail performance analysis of NRD T-branch power splitter at 60 GHz and broadband operation.

T-branch 60 GHz	Transmission [dB]		Reflection [dB]		BW
	LSM$_{01}$	LSE$_{01}$	LSM$_{01}$	LSE$_{01}$	[GHz]
BDEA	−3.01	−36.0	−37.8	−53.4	−−
BHSA	−3.04	−28.3	−23.7	−51.1	−−
BGA	−3.06	−22.3	−62.0	−48.5	−−
BFA	−3.11	−21.9	−19.5	−52.7	−−
BPSO	−4.11	−12.7	−9.3	−43.9	−−
Broadband	**Transmission [dB]**		**Reflection [dB]**		**BW**
T-branch	**LSM$_{01}$**	**LSE$_{01}$**	**LSM$_{01}$**	**LSE$_{01}$**	**[GHz]**
BDEA	−3.12	−19.7	−22.2	−56.4	4.0
BGA	−3.04	−31.5	−21.3	−55.0	4.0
BHSA	−3.15	−19.2	−21.0	−56.0	4.0
BFA	−3.43	−17.7	−12.2	−53.6	−−
BPSO	−3.69	−19.5	−9.12	−48.7	−−

25, 60 and 250 number of iterations. Due to structural limitations of T-branch guide, it is quite challenging for each optimization approach to achieve a desired property. Therefore, the performance of BPSO and BFA is not satisfactory. Successful optimizations achieved same device performance with broad bandwidth around 4 GHz in the frequency range of 58 GHz-62 GHz, but BHSA and BDEA are more efficient than BGA. The best optimal results obtained by BDEA are shown in Fig. 14. Furthermore, the performance detail of proposed NRD T-branch power splitter is summarized in Table 3.

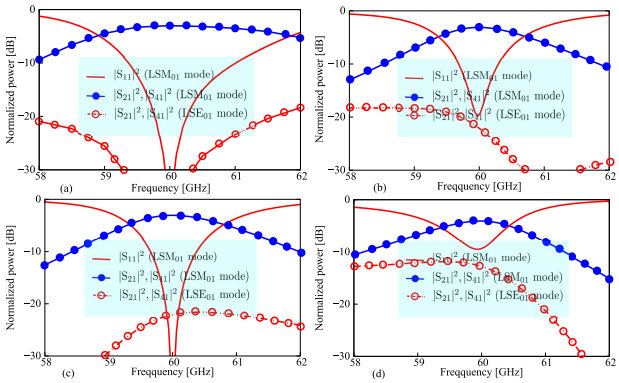

FIGURE 13. Frequency characteristics analysis of NRD T-branch at 60 GHz operation (a) BDEA (b) BFA (c) BGA (d) BPSO.

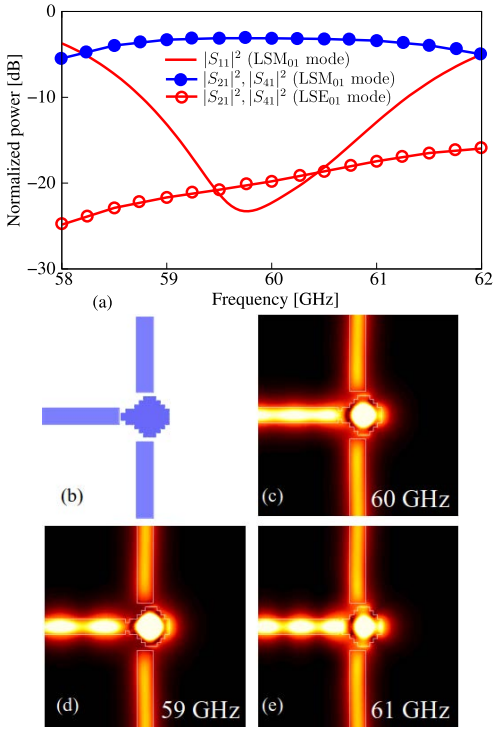

FIGURE 14. The frequency characteristics, optimized structure and propagation field of NRD T-branch power splitter at broadband operation using BDEA.

C. BENDING WAVEGUIDE

Next, we considered the third numerical example of an NRD bending waveguide as shown in Fig. 15. Except number of output ports, geometrical parameters and structural symmetrical conditions are the same as in the example of waveguide crossing. For maximum transmission, the following objective function is used at a single operating frequency.

$$\text{Minimize } F = 1 - |S_{21}(f)|^2 \quad \text{(at 60 GHz)} \tag{16}$$

where $|S_{21}|^2$ is the transmission power at port 2. Figure 16 (a) shows the convergence analysis of optimization approaches at 60 GHz in which BDEA, BHSA, BGA, and BFA achieving the best convergence results not more than 60 iterations but as usual GA require more iterations

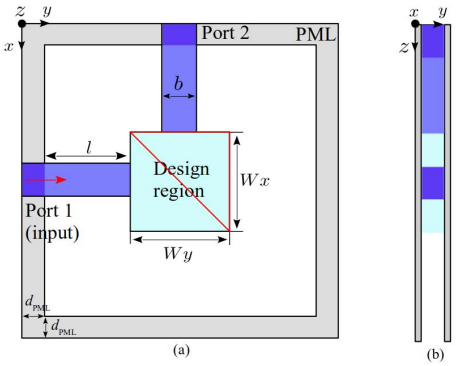

FIGURE 15. Initial structure of NRD bending waveguide (a) top view (b) front view.

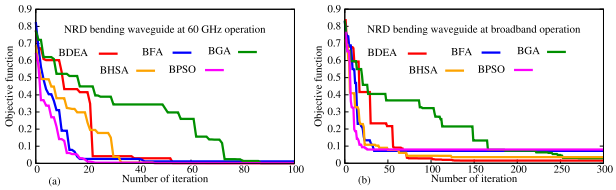

FIGURE 16. Convergence behavior of NRD bending waveguide at (a) 60 GHz (b) broadband operation.

confirmed in the previous example in both operation. Because of the sharp bending structure, it is challenging for each optimization approach to satisfy the desired properties. Figure 17 shows the optimal results of a bending waveguide at 60 GHz using BHSA. The frequency characteristics of bending waveguide using other optimizations are also shown in Fig. 18. As shown in Fig. 17 and 18, the structures obtained by BDEA, BHSA, BGA, BFA, and BPSO achieved high transmission power $|S_{21}|^2 = 0.998, 0.998, 0.999, 0.988$, and 0.998 respectively.

For broadband operation, we used the objective function as follow.

$$\text{Minimize } F = \frac{1}{3}\sum_{i=1}^{3}(1 - |S_{21}(f_i)|^2)$$
$$(f_{1,2,3} = 59,\ 60,\ 61 \text{ GHz}) \qquad (17)$$

The above objective function analyzes the guide structure using three frequencies 59, 60, 61 GHz. Figure 16(b) depicts the convergence behavior of a bending waveguide at broadband operation, with almost same convergence order to that of the preceding example of a broadband T-branch, where BDEA and BHSA are more efficient than BGA. BDEA, BHSA, and BGA achieved broad bandwidth about 3 GHz in this design example, while BPSO and BFA achieved 2.3 GHz and 2 GHz respectively. The best optimal results at broadband operation using BDEA are shown in Fig. 19. Furthermore, the performance detail of proposed NRD bending waveguide is summarized in Table 4.

D. FREQUENCY DEMULTIPLEXER

Finally, we consider another interesting example of NRD frequency demultiplexer whose initial structure, placement

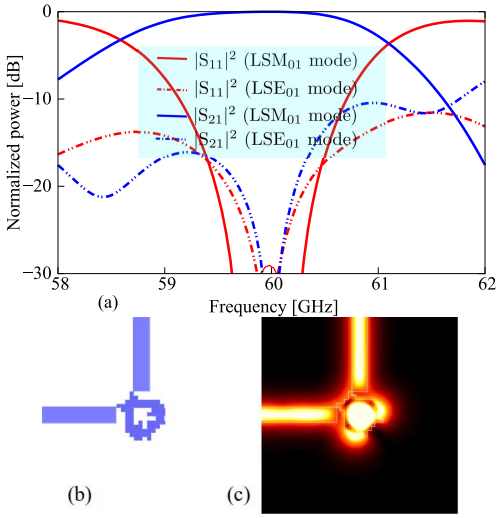

FIGURE 17. Optimal results of NRD bending at 60 GHz using BHSA (a) frequency characteristics, (b) optimized structure and (c) propagation field.

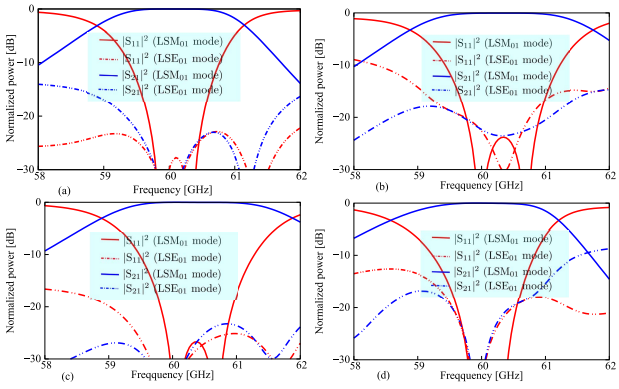

FIGURE 18. Frequency characteristics analysis of NRD bending at 60 GHz operation (a) BDEA (b) BFA (c) BGA (d) BPSO.

TABLE 4. Detail performance analysis of NRD bending waveguide at 60 GHz and broadband operation.

Bending 60 GHz	Transmission [dB]		Reflection [dB]		BW
	LSM$_{01}$	LSE$_{01}$	LSM$_{01}$	LSE$_{01}$	[GHz]
BGA	−0.003	−35.5	−34.7	−35.8	−−
BPSO	−0.004	−34.9	−33.9	−35.0	−−
BDEA	−0.006	−38.0	−29.8	−38.0	−−
BHSA	−0.007	−39.4	−29.1	−34.6	−−
BFA	−0.05	−22.6	−41.2	−22.3	−−
Broadband Bending	**Transmission [dB]**		**Reflection [dB]**		**BW**
	LSM$_{01}$	LSE$_{01}$	LSM$_{01}$	LSE$_{01}$	[GHz]
BDEA	−0.006	−38.0	−29.8	−38.0	3.0
BGA	−0.17	−31.8	−14.0	−33.5	3.0
BHSA	−0.007	−39.4	−29.1	−34.6	3.0
BFA	−0.14	−31.2	−14.1	−31.3	2.3
BPSO	−0.08	−21.0	−22.5	−22.2	2.0

of output ports, and incident conditions are different from those in the prior examples as shown in Fig. 20. It has one input and two output ports, as well as a design region of size 6 mm × 16 mm between them. The design region is divided into 12×32 pixels, with each of size is 0.5 mm × 0.5 mm. The gap between two output waveguides is set to be $d = 8$ mm

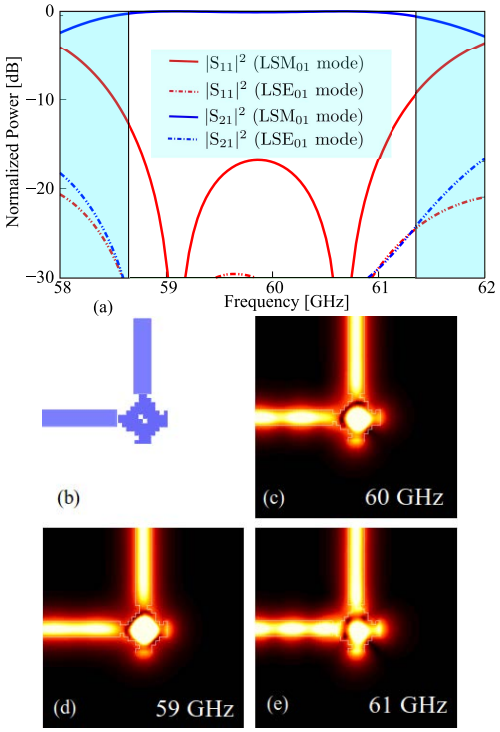

FIGURE 19. The frequency characteristics, optimized structure and propagation field of NRD bending waveguide at broadband operation using BDEA.

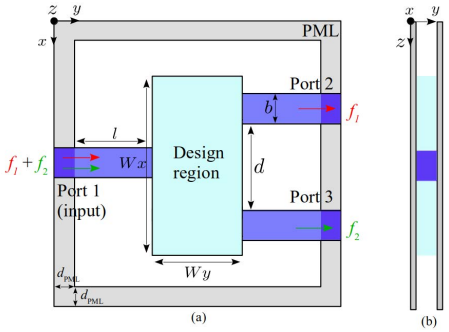

FIGURE 20. Initial structure of NRD frequency demultiplexer (a) top view (b) front view.

to avoid the coupling effect. To get the maximum power of a particular frequency at a desired output port, we ignore structural symmetry conditions in this case. Two frequencies $f_1 = 59$ GHz and $f_2 = 61$ GHz with LSM$_{01}$ mode are incident at input port 1 and are separated into two different output ports. The following objective function is used to separate the input frequencies.

$$\text{Minimize } F = \frac{1}{2}[(1 - |S_{21}(f_1)|^2) + (1 - |S_{31}(f_2)|^2)]$$
$$(f_{1,2} = 59,\ 61 \text{ GHz}) \tag{18}$$

where $|S_{21}|^2$ and $|S_{31}|^2$ are transmission powers at port 2 and port 3 for 59 GHz and 61 GHz respectively. After going through a design region optimized by using binary evolutionary approaches, two input frequencies are divided into two

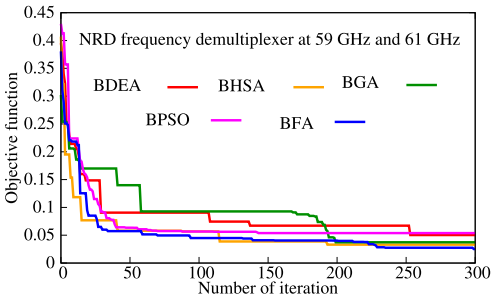

FIGURE 21. Convergence behavior of NRD frequency demultiplexer.

different output ports. The convergence trend of optimizations for designed device at 59 GHz and 61 GHz is shown in Fig. 21. In comparison to the preceding devices, more iterations are required for optimum convergence to obtain the desired properties due to complicated device functionality, multiple frequencies, and large size of design region. As demonstrated in Fig. 21, all optimization algorithms have a good enough convergence rate of less than 300 iterations. Figure 22 shows the best optimal results of the NRD frequency demultiplexer device using BFA. The frequency characteristics of the designed device is shown in Fig. 22 (a), with maximum transmission power at 59 GHz and 61 GHz, as indicated by the straight magenta line. At 59 GHz and 61 GHz, the transmission power is 0.964 and 0.985 with minimal crosstalk level 0.03 and 0.006 respectively. Figure 22(b) and (c) indicate that the propagation fields of 59 GHz and 61 GHz are fully guided into output waveguides without any coupling effect. The main purpose of the demultiplexer is to achieve multi-path interference in the design region. For 59 GHz operation, constructive interference occurs at output port 2 and destructive interference occurs at output port 3, and vice versa for 61 GHz operation. Figure 23 shows the frequency characteristics analysis of designed device utilizing various optimization approaches, which similarly obtained the desired transmission property of more than 0.95. Furthermore, the performance detail of proposed NRD frequency demultiplexer is summarized in Table 5.

The developed evolutionary approaches have a large degree of design freedom and require a small number of variables to efficiently optimize the pixel pattern in the design region. They result in high computation efficiency and converge the solution very quickly within a few iterations. This has been observed in proposed NRD guide devices. In addition, no matter how complex the device functionality and structure is or how large the design region is, developed evolutionary techniques are totally trustworthy for any type of NRD guide at single frequency operation. In spite of several practical advantages that are mentioned above, developed evolutionary approaches have some limitations too, the most important one being the careful selection of hyper parameters. Inappropriate parameter selection can result in population stagnation and premature convergence, rendering a solution unfeasible. Two of our five developed optimization approaches, BPSO and BFA, are not completely reliable in

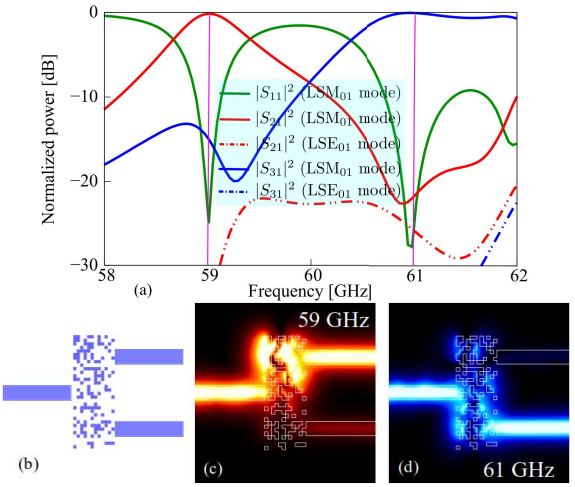

FIGURE 22. Optimal results of NRD frequency demultiplexer at 59 GHz and 61 GHz using BFA (a) frequency characteristics, (b) optimized structure and (c) propagation field at 59 GHz and (d) at 61 GHz.

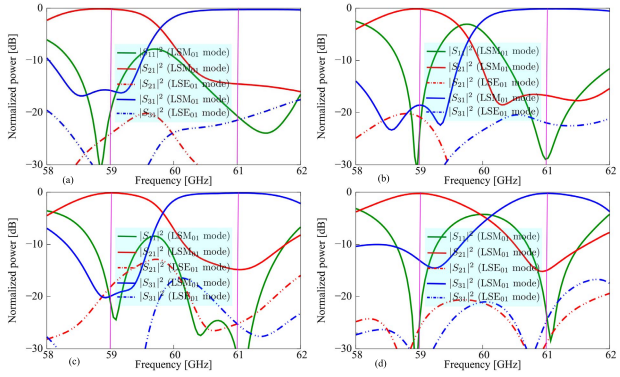

FIGURE 23. Frequency characteristics analysis of NRD frequency demultiplexer at 59 GHz and 61 GHz (a) BDEA (b) BHSA (c) BGA (d) BPSO.

TABLE 5. Detail performance analysis of NRD frequency demultiplexer at 59 GHz and 61 GHz.

Freq. Demux. 59 GHz	Transmission [dB]		Reflection [dB]		X-talk
	LSM_{01}	LSE_{01}	LSM_{01}	LSE_{01}	[dB]
BFA	−0.15	−37.3	−24.6	−31.9	−14.8
BHSA	−0.15	−20.8	−24.7	−19.6	−18.5
BGA	−0.15	−18.2	−20.8	−27.1	−19.9
BDEA	−0.32	−23.0	−15.1	−25.6	−14.4
BPSO	−0.24	−26.1	−25.4	−28.0	−13.0
Freq. Demux. 61 GHz	**Transmission [dB]**		**Reflection [dB]**		**X-talk**
	LSM_{01}	LSE_{01}	LSM_{01}	LSE_{01}	[dB]
BFA	−0.06	−42.2	−26.3	−24.7	−21.8
BHSA	−0.13	−21.9	−29.0	−26.2	−16.7
BGA	−0.17	−25.2	−31.2	−28.2	−14.8
BDEA	−0.38	−20.3	−16.4	−21.3	−13.3
BPSO	−0.23	−24.7	−22.8	−19.3	−15.0

broadband operation, which is a only limitation. On the other hand, BDEA, BHSA, and BGA, are extremely efficient in both operations.

In order to investigate the stability performance of our developed evolutionary approaches, we considered the NRD T-branch power splitter which is the most challenging device for developed optimizations has been proven above.

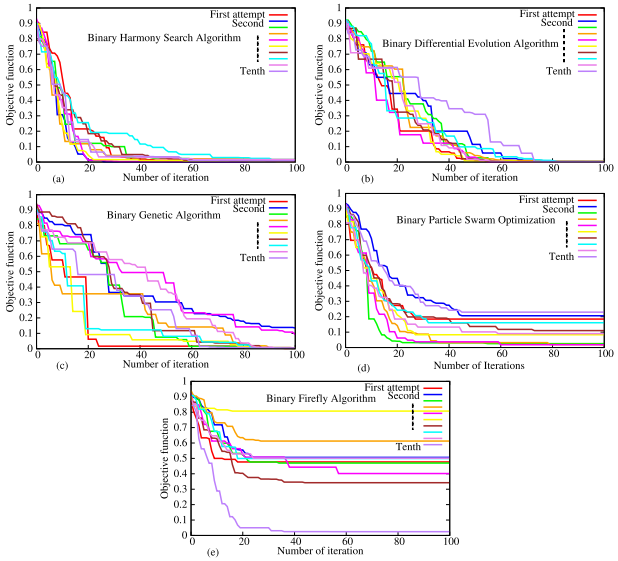

FIGURE 24. Stability analysis of developed evolutionary approaches (a) BHSA (b) BDEA (c) BGA (d) BPSO (e) BFA.

The device configuration, initialization and other hyper parameters of each optimization algorithm are same. The stability analysis is conducted by optimizing the considered device through ten attempts as shown in Fig. 24. We can see that BHSA and BDEA proves its high stability characteristics in each attempt but BHSA is more efficient than BDEA. The value of objective function in BGA is less than 0.2 with 100 iterations and may possible to achieve almost 0 with more iteration as obtained in BDEA and BHSA. The stability performance of BPSO and BFA is not impressive as achieved in rest of the optimizations. However, we can consider both of them for other simple NRD guide devices such as bending and crossing waveguide. Overall this analysis state that the BHSA is best one in term of stability, computational efficiency and reliability.

V. CONCLUSION

In this paper, we developed a set of evolutionary approaches using digital material concept for the efficient optimization of NRD guide devices. To reduce the computational efforts, originally developed 2D-FVFEM is used for the numerical simulations. Binary representation based GA, DEA, HSA, FA, and PSO are developed to efficiently optimize the material distribution in the design region of NRD guide devices. Four NRD circuit components including low crosstalk waveguide crossing, T-branch power splitter, bending waveguide and frequency demultiplexer are designed, and achieved high transmission throughput greater than 99.9%, 49.9%:49.9%, 99.9% at 60 GHz and 96.4%, 98.5% at 59 GHz and 61 GHz respectively. Furthermore, same devices except frequency demultiplexer are designed at broadband operation using modified objective function. Through comparative study we found that developed evolutionary approaches are highly efficient for single frequency operation. However,

it is quite challenging for broadband operation because of several frequencies in the objective function and structural limitation. We have achieved quite impressive results from proposed devices with minimal reflection and crosstalk level due to highly efficient optimization approaches. The proposed NRD guide devices may have a potential to realize a high-performance NRD based millimeter wave circuit. However, some improvements may possible to make optimization approaches more sophisticated for complex device functionalities. We are considering to design more interesting and efficient devices such as NRD-based isolators and circulators with attractive structural symmetrical conditions using developed evolutionary approaches.

REFERENCES

[1] T. Yoneyama and S. Nishida, "Nonradiative dielectric waveguide for millimeter-wave integrated circuits," *IEEE Trans. Microw. Theory Techn.*, vol. MTT-29, no. 11, pp. 1188–1192, Nov. 1981.

[2] T. Yoneyama and S. Nishida, "Nonradiative dielectric waveguide T-juctions for millimeter-wave application," *IEEE Trans. Microw. Theory Techn.*, vol. MTT-33, no. 11, pp. 1239–1241, Nov. 1985.

[3] T. Yoneyama, H. Tamaki, and S. Nishida, "Analysis and measurements of nonradiative dielectric waveguide bends," *IEEE Trans. Microw. Theory Techn.*, vol. MTT-34, no. 8, pp. 876–882, Aug. 1986.

[4] T. Yoneyama, "Millimeter-wave integrated circuits using nonradiative dielectric waveguide," *IEICE Trans. Electron. (Jananese Ed.)*, vol. J73-C, no. 3, pp. 87–94, Mar. 1990.

[5] F. Xu and K. Wu, "Substrate integrated nonradiative dielectric waveguide structures directly fabricated on printed circuit boards and metallized dielectric layers," *IEEE Trans. Microw. Theory Techn.*, vol. 59, no. 12, pp. 3076–3086, Dec. 2011.

[6] K. Wu and L. Han, "Hybrid integration technology of planar circuits and NRD-guide for cost-effective microwave and millimeter-wave applications," *IEEE Trans. Microw. Theory Techn.*, vol. 45, no. 6, pp. 946–954, Jun. 1997.

[7] F. Kuroki, K. Wada, and T. Yoneyama, "Low-loss and small-sized NRD guide ring resonators and their application to channel dropping filter at 60 GHz," *IEICE Trans. Electron.*, vol. E86-C, no. 8, pp. 1601–1606, Aug. 2003.

[8] D. Li, Y. Cassivi, P. Yang, and K. Wu, "Analysis and design of bridged NRD-guide coupler for millimeter-wave applications," *IEEE Trans. Microw. Theory Techn.*, vol. 53, no. 8, pp. 2546–2551, Aug. 2005.

[9] E. Polat, R. Reese, M. Jost, C. Schuster, M. Nickel, R. Jakoby, and H. Maune, "Tunable liquid crystal filter in nonradiative dielectric waveguide technology at 60 GHz," *IEEE Microw. Wireless Compon. Lett.*, vol. 29, no. 1, pp. 44–46, Jan. 2019.

[10] F. Kuroki, M. Kimura, Y. Murata, and T. Yoneyama, "A compact-sized NRD guide single mixer using band-pass filters at 60 GHz," in *IEEE MTT-S Int. Microw. Symp. Dig.*, Jun. 2005, pp. 2091–2094.

[11] F. Kuroki, A. Miyamae, and T. Yoneyama, "Flexible transmission line using high permittivity LSE-NRD guide at 60 GHz," *IEICE Trans. Electron*, vol. 87, no. 12, pp. 7–2195, Dec. 2004.

[12] F. Kuroki, S. Siunke, and T. Yoneyama, "Modeling of NRD guide beam lead diode devices for millimeter-wave applications," in *Proc. 11th IEEE Int. Symp. Electron Devices Microw. Optoelectron. Appl. (EDMO)*, Nov. 2003, pp. 229–233.

[13] F. Kuroki, S. Nakamura, T. Fukuchi, and T. Yoneyama, "NRD guide pin diode devices for automotive radar at 77 GHz," *IEICE Trans. Electron.*, vol. 86, no. 2, pp. 199–205, Feb. 2003.

[14] F. Kuroki, S. Shinke, E. Suematsu, H. Sato, and T. Yoneyama, "Wireless multi-channel TV-signal distribution system by using NRD guide transmitter and receiver at 60 GHz," in *IEEE MTT-S Int. Microw. Symp. Dig.*, May 2001, pp. 1813–1816.

[15] F. Kuroki, M. Sugioka, S. Matsukawa, K. Ikeda, and T. Yoneyama, "High-speed ASK transceiver based on the NRD-guide technology at 60-GHz band," *IEEE Trans. Microw. Theory Techn.*, vol. 46, no. 6, pp. 806–810, Jun. 1998.

[16] F. Kuroki, K. Ikeda, M. Sugioka, S. Matsukara, and T. Yoneyama, "High speed PCM transceiver based on the NRD guide technologies at 60 GHz band," in *Proc. Millim. Waves, Top. Symp.*, Jul. 1997, pp. 119–122.

[17] F. Kuroki, Y. Murata, and T. Yoneyama, "A filter-based NRD-guide duplexer with low-loss and high-isolation for wireless broad-band asymmetric digital subscriber line at 60 GHz," in *Proc. IEEE 34th Eur. Microw. Conf.*, vol. 3, Oct. 2004, pp. 1281–1284.

[18] T. Bashir, K. Morimoto, A. Iguchi, Y. Tsuji, and T. Kashiwa, "Optimal design of 90°-bend in NRD guide using DBS algorithm and 2D-FVFEM," in *Proc. IEEE Int. Symp. Antennas Propag. USNC-URSI Radio Sci. Meeting (APS/URSI)*, Dec. 2021, pp. 1643–1644.

[19] T. Bashir, K. Morimoto, A. Iguchi, Y. Tsuji, T. Kashiwa, and S. Nishiwaki, "Optimal design of NRD guide devices using 2D full-vectorial finite element method," *IEICE Electron. Exp.*, vol. 18, no. 15, Aug. 2021, Art. no. 20210243.

[20] T. Bashir, K. Morimoto, A. Iguchi, Y. Tsuji, T. Kashiwa, and S. Nishiwaki, "Optimal design of broadband non-radiative dielectric guide devices using binary genetic algorithm and 2D-FVFEM," *Int. J. Numer. Model., Electron. Netw., Devices Fields*, to be published, doi: 10.1002/jnm.2984.

[21] F. Boone and K. Wu, "Mode conversion and design consideration of integrated nonradiative dielectric (NRD) components and discontinuities," *IEEE Trans. Microw. Theory Techn.*, vol. 48, no. 4, pp. 482–492, Apr. 2000.

[22] J. Dallaire and K. Wu, "Complete characterization of transmission losses in generalized nonradiative dielectric (NRD) waveguide," *IEEE Trans. Microw. Theory Techn.*, vol. 48, no. 1, pp. 121–125, Jan. 2000.

[23] T. Yoneyama, N. Tozawa, and S. Nishida, "Loss measurements of nonradiative dielectric waveguide (special papers)," *IEEE Trans. Microw. Theory Techn.*, vol. MTT-32, no. 8, pp. 943–946, Aug. 1984.

[24] J. Y. Lee, J. H. Lee, C. H. Im, H. S. Kim, K. Choi, and H. K. Jung, "Selection of proper modes of an NRD guide using a perturbing boundary," *IEEE Trans. Magn.*, vol. 39, no. 3, pp. 1246–1249, May 2003.

[25] K. Maamria, T. Wagatsuma, and T. Yoneyama, "Leaky NRD guide as a feeder for microwave planar antennas," *IEEE Trans. Antennas Propag.*, vol. 41, no. 12, pp. 1680–1686, Dec. 1993.

[26] F. Kuroki, K. Makoto, and T. Yoneyama, "Transition between NRD guide and microstrip line at 60 GHz," *IEICE Trans. Electron.*, vol. E88-C, no. 10, pp. 1968–1972, Oct. 2005.

[27] Y. Kamo, K. Munetou, and F. Kuroki, "Transmission loss evaluation of 94GHz NRD guide toward THz-band dielectric integrated circuits," in *Proc. IEEE Int. Symp. Radio-Freq. Integr. Technol. (RFIT)*, Aug. 2016, pp. 1–3.

[28] K. Wu, "A combined efficient approach for analysis of nonradiative dielectric (NRD) waveguide components," *IEEE Trans. Microw. Theory Techn.*, vol. 42, no. 4, pp. 672–677, Apr. 1994.

[29] U. Schmid and W. Menzel, "A 24 GHz microstrip antenna array with a nonradiative dielectric waveguide (NRD-guide) feeding network," in *Proc. 11th Int. Symp. Antenna Technol. Appl. Electromagn. (ANTEM)*, Jun. 2005, pp. 1–4.

[30] F. Kuroki, H. Ohta, and T. Yoneyama, "Transmission characteristics of NRD guide as a transmission medium in THz frequency band," *IEEE 30th Int. Conf. Infr. Millim. Waves 13th Int. Conf. THz Electron.*, vol. 2, pp. 331–332, Sep. 2005.

[31] F. Kuroki, M. Kimura, and T. Yoneyama, "Analytical study on guided modes in vertical strip line embedded in NRD guide," *Electron. Lett.*, vol. 40, no. 18, pp. 1121–1122, Sep. 2004.

[32] F. Kuroki, M. Yamaguchi, Y. Minamitani, and T. Yoneyama, "High permittivity LSE-NRD guide and its application to a new type of millimeter wave antenna," *IEICE Trans. Electron.*, vol. 86, no. 2, pp. 169–175, Feb. 2003.

[33] D. Marcuse, "Length optimization of an S-shaped transition between offset optical waveguides," *Appl. opt.*, vol. 17, no. 5, pp. 763–768, Mar. 1978.

[34] J. Byun and I. Park, "Design of dielectric waveguide filters using topology optimization technique," *IEEE Trans. Magn.*, vol. 43, no. 4, pp. 15–73, Mar. 2007.

[35] A. Iguchi, Y. Tsuji, T. Yasui, and K. Hirayama, "Efficient topology optimization of optical waveguide devices utilizing semi-vectorial finite-difference beam propagation method," *Opt. Exp.*, vol. 25, no. 3, pp. 28210–28222, Nov. 2017.

[36] A. Iguchi, Y. Tsuji, T. Yasui, and K. Hirayama, "Topology optimization of optical waveguide devices based on beam propagation method with sensitivity analysis," *J. Lightw. Technol.*, vol. 34, no. 18, pp. 4220–5214, Sep. 15, 2016.

[37] A. Iguchi, Y. Tsuji, T. Yasui, and K. Hirayama, "Efficient shape and topology optimization based on sensitivity analysis for optical waveguide devices utilizing full-vectorial BPM," *J. Lightw. Technol.*, vol. 38, no. 8, pp. 2328–2335, Apr. 15, 2020.
[38] A. Koda, K. Morimoto, and Y. Tsuji, "A study on topology optimization of plasmonic waveguide devices using function expansion method and evolutionary approach," *J. Lightw. Technol.*, vol. 37, no. 3, pp. 981–988, Feb. 1, 2019.
[39] J.-H. Jung, "Optimal design of dielectric-loaded surface plasmon polariton waveguide with genetic algorithm," *J. Opt. Soc. Korea*, vol. 14, no. 3, pp. 277–281, Sep. 2010.
[40] L. Sanchis, A. Håkansson, D. López-Zanón, J. Bravo-Abad, and J. Sánchez-Dehesa, "Integrated optical devices design by genetic algorithm," *Appl. Phys. Lett.*, vol. 84, no. 22, pp. 4460–4462, May 2004.
[41] R. Coccioli, G. Pelosi, and S. Selleri, "Optimization of bends in rectangular waveguide by a finite-element genetic-algorithm procedure," *Microw. Opt. Technol. Lett.*, vol. 16, no. 5, pp. 287–290, Dec. 1997.
[42] J. Jung, "Optimal design of plasmonic waveguide using multiobjective genetic algorithm," *Opt. Eng.*, vol. 55, no. 1, Jan. 2016, Art. no. 017103.
[43] R. Shiratori, M. Nakata, K. Hayashi, and T. Baba, "Particle swarm optimization of silicon photonic crystal waveguide transition," *Opt. Lett.*, vol. 46, no. 8, pp. 1904–1907, Apr. 2021.
[44] J. C. Mak, C. Sideris, J. Jeong, A. Hajimiri, and J. K. Poon, "Binary particle swarm optimized 2×2 power splitters in a standard foundry silicon photonic platform," *Opt. lett.*, vol. 41, no. 16, pp. 3868–3871, Aug. 2016.
[45] W. Chen, B. Zhang, P. Wang, S. Dai, W. Liang, H. Li, Q. Fu, J. Li, Y. Li, T. Dai, and H. Yu, "Ultra-compact and low-loss silicon polarization beam splitter using a particle-swarm-optimized counter-tapered coupler," *Opt. Exp.*, vol. 28, no. 21, pp. 30701–30709, Oct. 2020.
[46] T. Fujisawa and K. Saitoh, "Ultrasmall two-mode dividers based on mosaic structure designed by direct-binary-search algorithm aided by artificial neural network," in *Proc. Opto-Electron. Commun. Conf. (OECC)*, Oct. 2020, pp. 1–3.
[47] T. Fujisawa and K. Saitoh, "Bayesian direct-binary-search algorithm for the efficient design of mosaic-based power splitters," *OSA Continuum*, vol. 4, no. 4, pp. 1258–1270, Apr. 2021.
[48] W. Chang, L. Lu, X. Ren, D. Li, Z. Pan, M. Cheng, D. Liu, and M. Zhang, "Ultracompact dual-mode waveguide crossing based on subwavelength multimode-interference couplers," *Photon. Res.*, vol. 6, no. 7, pp. 660–665, Jul. 2018.
[49] Y. Xu, H. Ma, T. Xie, J. Yang, and Z. Zhang, "Ultra-compact power splitters with low loss in arbitrary direction based on inverse design method," *Photonics*, vol. 8, no. 11, pp. 516–526, Nov. 2021.
[50] W. Chang, L. Lu, X. Ren, L. Lu, M. Cheng, D. Liu, and M. Zhang, "An ultracompact multimode waveguide crossing based on subwavelength asymmetric Y-junction," *IEEE Photon. J.*, vol. 10, no. 4, pp. 1–8, Aug. 2018.
[51] Y. Tsuji, K. Morimoto, A. Iguchi, T. Kashiwa, and S. Nishiwaki, "Two-dimensional full-vectorial finite element analysis of NRD guide devices," *IEEE Microw. Wireless Compon. Lett.*, vol. 31, no. 4, pp. 345–348, Apr. 2021.
[52] J. H. Holland, *Adaptation in Natural and Artificial Systems*," Ann Arbor, MI, USA: Univ. Michigan Ann Arbor, 1992.
[53] R. Storn and K. Price, "Differential evolution—A simple and efficient heuristic for global optimization over continuous spaces," *J. Glob. Optim.*, vol. 11, no. 4, pp. 341–359, Dec. 1997.
[54] Z. W. Geem, J. H. Kim, and G. V. Loganathan, "A new heuristic optimization algorithm: Harmony search," *J. Simul.*, vol. 76, no. 2, pp. 60–68, Feb. 2001.
[55] R. Eberhart and J. Kennedy, "A new optimizer using particle swarm theory," in *Proc. Micro Mach. Hum. Sci.*, Apr. 1995, pp. 39–43.
[56] X.-S. Yang, "Firefly algorithms for multimodal optimization," in *Proc. Int. Symp. (SAGA)*, Sapporo, Japan, Oct. 2009, pp. 169–178.

TAHIR BASHIR (Graduate Student Member, IEEE) received the B.Sc. degree in telecommunication engineering from the Islamia University of Bahawalpur, Pakistan, in 2018, and the M.S. degree in electronics and communication engineering from Chongqing University, Chongqing, China, in 2020. He is currently pursuing the Ph.D. degree in information and electronics engineering with the Muroran Institute of Technology, Muroran, Japan. He is a Student Member of the Institute of Electronics, Information and Communication Engineers (IEICE).

KEITA MORIMOTO (Member, IEEE) received the B.S., M.S., and Ph.D. degrees in information and electronic engineering from the Muroran Institute of Technology, Muroran, Japan, in 2017, 2019, and 2021, respectively. From April 2021 to March 2022, he was a Postdoctoral Research Fellow with the Japan Society for the Promotion of Science (JSPS). He is currently an Assistant Professor at the University of Hyogo. He is a member of the Institute of Electronics, Information and Communication Engineers (IEICE).

AKITO IGUCHI (Member, IEEE) received the B.S., M.S., and Ph.D. degrees in electronic engineering from the Muroran Institute of Technology, Muroran, Japan, in 2015, 2017, and 2019, respectively. From 2019 to 2020, he was a Postdoctoral Research Fellow with the Japan Society for the Promotion of Science (JSPS). He is currently an Assistant Professor at the Muroran Institute of Technology. He is a member of the Institute of Electronics, Information and Communication Engineers (IEICE).

YASUHIDE TSUJI (Senior Member, IEEE) received the B.S., M.S., and Ph.D. degrees in electronic engineering from Hokkaido University, Sapporo, Japan, in 1991, 1993, and 1996, respectively. In 1996, he joined the Department of Applied Electronic Engineering, Hokkaido Institute of Technology, Sapporo. From 1997 to 2004, he was an Associate Professor of electronics and information engineering at Hokkaido University. From 2004 to 2011, he was an Associate Professor of electrical and electronic engineering at the Kitami Institute of Technology, Kitami, Japan. Since 2011, he has been a Professor of information and electronic engineering at the Muroran Institute of Technology, Muroran, Japan. His research interest includes wave electronics. He is a Senior Member of the Institute of Electronics, Information and Communication Engineers (IEICE) and a member of the Japan Society of Applied Physics and the Optical Society of America (OSA). In 1997, 1999, and 2019, he was awarded the Best Paper Award from IEICE. In 2000, he has received the Third Millennium Medal from IEEE. In 2019, he has received the IEEE Photonics Technology Letters Outstanding Reviewer Award.

TATSUYA KASHIWA (Senior Member, IEEE) was born in Hokkaido, Japan, in 1961. He received the B.S., M.S., and Ph.D. degrees in electrical engineering from Hokkaido University, Sapporo, Japan, in 1984, 1986, and 1988, respectively. In 1988, he joined the Department of Electrical Engineering, Hokkaido University, as an Assistant Professor. In 1996, he joined the Department of Electrical and Electronic Engineering, Kitami Institute of Technology, as an Associate Professor, where he has been a Professor, since 2008. He has coauthored the books *Handbook of Microwave Technology* (Academic Press), *Antennas and Associated Systems for Mobile Satellite Communications* (Research Signpost), and *Antennas for Small Mobile Terminals* (Artech House). His research interests include the analysis of electromagnetic and acoustic fields, electromagnetic compatibility, and optimization problems. He is a member of IEEJ and a fellow of IEICE. He is a member of the Technical Committee on Electromagnetic Theory and Microwaves of IEICE. He was a recipient of the IEEE APS Tokyo Chapter Young Engineer Award in 1992 and the IEEJ Technical Development Award in 2019. He was the Chairperson of the Technical Committee on Electronics Simulation Technology.